Int. J. Exp. Path. (2008), 89, 419–432
doi: 10.1111/j.1365-2613.2008.00608.x

ORIGINAL ARTICLE

An intravital microscopic study of the hepatic microcirculation in cirrhotic mice models: relationship between fibrosis and angiogenesis

Eline Vanheule*,[1], Anja M. Geerts*,[1], Jacques Van Huysse†, Daphné Schelfhout*, Marleen Praet†, Hans Van Vlierberghe*, Martine De Vos* and Isabelle Colle*

**Department of Hepatology and Gastroenterology, Ghent University Hospital, Ghent, Belgium and †Department of Pathology, Ghent University Hospital, Ghent, Belgium*

INTERNATIONAL JOURNAL OF EXPERIMENTAL PATHOLOGY

Summary

This intravital fluorescence microscopy (IVFM) study validates cirrhotic mice models and describes the different intrahepatic alterations and the role of angiogenesis in the liver during genesis of cirrhosis. Cirrhosis was induced by *subcutaneous* injection of carbon tetrachloride (CCl_4) and by common bile duct ligation (CBDL) in mice. Diameters of sinusoids, portal venules (PV), central venules (CV) and shunts were measured at different time points by IVFM. Thereafter, liver samples were taken for sirius red, CD31, Ki67, vascular endothelial growth factor (VEGF) and α-smooth muscle actin (α-SMA) evaluation by immunohistochemistry (IHC). In parallel with fibrogenesis, hepatic microcirculation was markedly disturbed in CCl_4 and CBDL mice with a significant decrease in sinusoidal diameter compared to control mice. In CCl_4 mice, CV were enlarged, with marked sinusoidal-free spaces around CV. In contrast, PV were enlarged in CBDL mice and bile lakes were observed. In both mice models, intrahepatic shunts developed gradually after induction. During genesis of cirrhosis using CD31 IHC we observed a progressive increase in the number of blood vessels within the fibrotic septa area and a progressively increase in staining by Ki67, VEGF and α-SMA of endothelial cells, hepatocytes and hepatic stellate cells respectively. *In vivo* study of the hepatic microcirculation demonstrated a totally disturbed intrahepatic architecture, with narrowing of sinusoids in both cirrhotic mice models. The diameters of CV and PV increased and large shunts, bypassing the sinusoids, were seen after both CCl_4 and CBDL induction. Thus present study shows that there is angiogenesis in the liver during cirrhogenesis, and this is probably due partially to an increased production of VEGF.

Keywords
angiogenesis, cirrhosis, hepatic microcirculation, intravital microscopy, mice models

Received for publication:
1 October 2007
Accepted for publication:
18 June 2008

Correspondence:
Eline Vanheule
Department of Hepatology and Gastroenterology
Ghent University Hospital, building K12 first floor IE
De Pintelaan 185
9000 Ghent
Belgium
Tel.: +32 9 3322371
Fax: +32 9 3324984
E-mail: eline.vanheule@UGent.be

[1]Both the authors contributed equally to this work.

Cirrhosis is a worldwide frequent disease associated with a high mortality and morbidity. It can be defined as a diffuse process characterized by fibrosis and the conversion of normal liver architecture into structurally abnormal nodules (Anthony *et al.* 1977). The pathological process in the development of cirrhosis consists of a complex network of interacting cells, fibrogenic mediators and extracellular matrix molecules (Gressner 1992; Gressner & Bachem 1995). Besides these molecular aspects in the process of fibrogenesis, alterations in the hepatic vasculature are also defined as a crucial component in the development of the cirrhotic state (Schaffner & Poper 1963; Popper 1977; Rappaport *et al.* 1983). As early as 1963, Schaffner & Poper described the presence of a capillary basement membrane and loss of sinusoidal endothelial cell fenestrations in the cirrhotic liver, calling this phenomenon capillarization of hepatic sinusoids (Schaffner & Poper 1963). In addition, other microvascular abnormalities such as shunts between pre- and postsinusoidal vessels were observed (Gaudio *et al.* 1993; Vollmar *et al.* 1998; Onori *et al.* 2000). The development of shunts involves either the opening of preformed channels or the formation of new vessels, angiogenesis (Rappaport *et al.* 1983). Angiogenesis has been shown to play an important role in the development of liver fibrosis (El-Assal *et al.* 1998; Yoshiji *et al.* 2003) and involves a tightly regulated network of cellular and molecular mechanisms that result in the formation of functional vessels. Of particular importance are growth factors [e.g. vascular endothelial growth factor (VEGF), hepatocyte growth factor (HGF), transforming growth factor-β (TGF-β)] involved in matrix-remodelling and cell migration. HGF is a powerful inducer of angiogenesis (Camussi *et al.* 1997; Rosen *et al.* 1997) and can be amplified by other growth factors (Silvagno *et al.* 1995). TGF-β stimulates most of the processes of wound healing in collaboration with other growth factors, such as VEGF, and is a major profibrotic factor known for activated hepatic stellate cells (HSC) (Hyytiainen *et al.* 2004; Ruiz-Ortega *et al.* 2007). In this study, we will focus on VEGF, which is considered as one of the key mediators for new blood vessel formation in physiological and pathological conditions (Carmeliet 2005).

Intravital fluorescence microscopy (IVFM) of the liver is used to study the *in vivo* structural changes at microcirculatory level during cirrhogenesis. This technique has the advantage, in comparison with traditionally used scanning electron microscopy, to study dynamic alterations in the hepatic microcirculation.

Carbon tetrachloride (CCl_4) administration and common bile duct ligation (CBDL) are two widely used animal models to study the pathological intrahepatic changes related to cirrhosis. So far, the most common animal used for these experiments is the rat (Proctor & Chatamra 1982; Perez Tamayo 1983; Kountouras *et al.* 1984; Vorobioff *et al.* 1984; Lee *et al.* 1986a,b; Colombato *et al.* 1992; Castaneda *et al.* 2000; Katsuta *et al.* 2005). However, with the advances in molecular biology and the use of genetically modified animals (e.g. transgenic or knock-out mice), well-described models in mice are needed. Recently, we were able to make a characterization of a *subcutaneously* induced CCl_4 and CBDL model in mice (Geerts AM, Vanheule E, Praet M, Van Vlierberghe H, De Vos M, Colle I, 2008, unpublished data). Hepatic microcirculatory observations with the use of IVFM has been described in the literature in intraperitoneal-induced CCl_4 mice models (Niggemann *et al.* 2004), but data about alterations of hepatic circulation after bile duct ligation and *subcutaneous* CCl_4 induction in mice are not available.

The present study was performed to validate two mice models of cirrhosis *in vivo* with IVFM. We evaluated and compared different parameters of the hepatic microcirculation during the development of fibrosis/cirrhosis in a *subcutaneously* induced CCl_4 mice model and in a mice model of biliary cirrhosis, induced by CBDL. In correlation with our results *in vivo*, we determined the role of angiogenesis during the process of fibrosis and cirrhosis in both models. A better knowledge about angiogenesis can give more opportunities to develop new therapeutic strategies that target the process of fibrosis and cirrhosis.

Materials and methods

The experiments were performed in male Swiss albino mice (20–25 g) (strain HsdWin: CFW-1) purchased from Harlan laboratories (Horst, the Netherlands). The mice were kept under constant temperature and humidity in a 12 h controlled dark/light cycle. The Ethical Committee of experimental animals at the Faculty of Medicine and Health Sciences, Ghent University, Belgium, approved the protocols.

Mice model of CCl_4 induced cirrhosis

Carbon tetrachloride (Merck, Darmstadt, Germany) was administrated by dorsal *subcutaneous* injection (1:1 dissolved in olive oil; 1 ml/kg) twice weekly. Five percent alcohol was added to their drinking water. Hepatic necrosis by CCl_4 is intensified when cytochrome P450 2E1 enzyme is induced by administration of ethanol (Koop & Coon 1986; Koop & Tierney 1990). Experiments were performed 3 days after the last CCl_4 administration. Control mice received pure olive oil (1 ml/kg) *subcutaneously* twice weekly and no ethanol was added to their drinking water.

The mice were killed after 4, 8, 10, 12 and 16 weeks of CCl_4 administration or pure olive oil (n = 6 in each group).

Mice model of secondary biliary cirrhosis

Secondary biliary cirrhosis was induced by CBDL. Under isoflurane inhalation anaesthesia, a midline abdominal incision was made and the common bile duct was isolated from the surrounding tissue. The common bile duct was occluded with a double ligature of a non-resorbable suture (silk cut 5-0). The first ligature was made below the junction of the hepatic ducts and the second was made above the entrance of the pancreatic duct. The common bile duct was resected between the two ligatures. The abdominal wall was closed by suturing abdominal muscle and skin (silk cut 5-0).

Control mice were sham-operated, the abdominal cavity was opened and the common bile duct was isolated, but no ligature was placed. The mice were killed 1, 3 and 6 weeks after CBDL or sham-operation (n = 6 in each group).

IVFM of the liver

Surgical preparation. The intravital microscope and the surgical preparation is shown in Figure 1. Mice were fastened overnight and anaesthetized with a mixture of ketamine (Ketalar®, 50 mg/ml, Pfizer, Brussels, Belgium) and xylazine (Rompun® 2%, 20 mg/ml, Bayer, Brussels, Belgium), administered *subcutaneously* in a dose of 100 and 10 respectively. An intravenous catheter was inserted into the jugular vein for continuous infusion of saline and fluorescent dyes. Thereafter, a midline and left subcostal incision was made so as to exteriorise the liver. The hepatic ligaments were dissected and the intestine was covered with a saline-soaked gauze to minimize tissue dehydratation. The mice were placed in a left supine position on a heating pad for maintenance of body temperature at 37 °C. The left liver lobe was then exteriorised and placed on a plasticine disk that was attached to the heating pad. Subsequently, the lower surface of the liver was situated horizontal to the microscope and the plasticine disk minimized the respiratory movements of the lobe. The exposed area of the left liver lobe was immediately covered with a glass slide to prevent drying of the tissue.

Intravital fluorescence microscopy. By use of a modified fluorescence Axiotech Vario 100 HD microscope (Zeiss, Jena, Germany), with a 50-W HBO mercury lamp attached to an UV, green and blue filter system, the hepatic microcirculation was analysed using epi-illumination (Vollmar *et al.* 1998). With the use of a 10× objective (10×/0.30 W, Zeiss) and a 20× objective (20×/0.45 W, Zeiss), images were displayed on a television monitor by a TK-1281 (Victor Company of Japan LTD-JVC, Tokyo, Japan) and recorded by a video recorder (S-VHS Panasonic AG-7350, Matsushita, Japan) for off-line analysis. The video images were analysed with an image analysis software program (CAP-IMAGE, Ingenieursbüro Zeintl, Heidelberg, Germany).

The structure of the hepatic microcirculation was analysed after tissue contrast enhancement by intravenous injection of sodium fluorescein (2 μmol/kg intravenous, Sigma, Bornem, Belgium) using blue light epi-illumination (450–490 nm/>520 nm, excitation/emission wavelength). HSC were visualised by auto-fluorescence of vitamin A using an UV filter system (330–380 nm/>415 nm, excitation/emission wavelength), which were completely eliminated after approximately 20 s because of their rapid photo bleaching property (Suematsu *et al.* 1993).

Quantitative offline analysis. The sinusoids, central venules (CV), portal venules (PV) and shunt diameters were analysed in each mouse. The duration of the IVFM experiment for each mouse was maximum 60 min.

A liver acinus is subdivided into three circulatory zones (Rappaport *et al.* 1983):

Zone 1: area where terminal portal afferent branches empty into sinusoids and where arterial and portal stream mix. This is the zone close to the supplying vessels and portal tracts.

Zone 2: this area can be defined as the remaining zone between 1 and 3.

Zone 3: area close to a terminal hepatic venule and CV. The cells in zone 3 are most sensitive to damage through ischaemia, anoxia, congestion and nutritional deficiency.

The sinusoidal diameters were analysed in five sinusoids in zone 2 of an acinus, and 20 acini were studied in each mouse.

Mean arterial blood pressure and portal pressure measurement

At the beginning of the experiment, mean arterial pressure (MAP) and at the end of the experiment portal pressure (PP) was measured in each mouse to evaluate portal hypertension. The carotid artery was cannulated for monitoring the mean arterial blood pressure. In addition, the portal vein was cannulated through an ileocolic vein with a 24-gauge catheter (Becton Dickinson, Erembodegem-Aalst, Belgium), which was advanced into the portal vein and connected to a highly sensitive pressure transducer. The external zero reference

point was placed at the midportion of the animal. The measurements were recorded on a multi-channel computer-based recorder (Powerlab, ADInstruments, Spechbach, Germany).

Histopathology of the liver

After IVFM and haemodynamic measurements, the mice were sacrificed. Samples of the liver were fixed in 4% phosphate-buffered formaldehyde solution (Sigma, Bornem, Belgium) and embedded in paraffin. From all tissue samples, 2 μm tissue sections were cut with a Leica RM 2145 sliding microtome (Leica Microsystems, Nussloch, Germany) for histology.

Sirius red staining. Sirius red staining results in a red staining of all fibrillary collagen and is used to evaluate the stage of fibrosis/cirrhosis. The liver tissue sections were stained with 0.1% picrosirius red (Klinipath, Geel, Belgium).

CD31 immunohistochemistry. CD31 staining, a marker for endothelial cells, was performed to evaluate the number of blood vessels (Fernandez *et al.* 2004; Carmeliet 2005). Liver sections were deparaffinized, rehydrated and incubated for 7 min with trypsin (Sigma, Bornem, Belgium) on 37 °C. Thereafter, endogenous peroxidase was blocked for 20 min with hydrogen peroxidase (VWR, Leuven, Belgium) in methanol. Subsequently, they were overnight incubated at room temperature with primary antibody rat anti-mouse CD31 (1/500, MEC 13.3, ref: 550274, BD Pharmingen, BD Bioscience, Erembodegem, Belgium) and thereafter for 1 h at room temperature with secondary rabbit anti-rat biotinylated antibody (1/300, ref: EO468, Dako cytomation, Heverlee, Belgium). The specificity of the immunolabelling was confirmed by incubation without primary antibody. Further, streptavidin-biotinylated links (TSA Biotin System, Perkin Elmer, Boston, MA, USA) were applied. 3, 3′ diaminobenzidine (DAB kit; Dako Cytomation, Heverlee, Belgium) was used as chromogenic substrate to visualize immunolabelling, resulting in a brown precipitate.

Ki67 Immunohistochemistry. Ki67 staining, a marker for proliferating cells, was used to evaluate proliferating endothelial cells. Ki67 staining used the Ventana system (Ventana Medical Systems Inc., Tucson, AZ, USA). After deparaffinization, liver sections were treated sequentially with inhibitor for 4 min. Then, the sections were incubated with rabbit monoclonal Ki67 antibody (clone SP6, ref: RM-9106-R7, Neo Markers, Lab vision, CA, USA) for 30 min, after which they were incubated sequentially with amplifier A, amplifier B, biotinylated immunoglobulin, avidin–horseradish peroxidase, DAB and DAB H_2O_2 for 8 min each. The sections were counterstained with haematoxylin for 6 min and with bluing reagent for 2 min. All steps were performed at 37 °C.

VEGF immunohistochemistry. Vascular endothelial growth factor, one of the proteins responsible for angiogenesis, was performed by immunohistochemistry (IHC). Liver sections were deparaffinized, rehydrated and incubated in triphosphate buffered saline with hydrogen peroxidase (VWR, Leuven, Belgium) and sodium azide for 20 min to block endogenous peroxidase. Subsequently, they were incubated for 1 h at room temperature with primary antibody rabbit anti-mouse VEGF (VEGF A-20, sc-152; Santa Cruz Biotechnology, Santa Cruz, CA, USA) at a concentration of 1/250. The specificity of the immunolabelling was confirmed by incubation without primary antibody. Thereafter, streptavidin-biotinylated links with the secondary antibody (LSAB + system-HRP, Dako Cytomation, Heverlee, Belgium) were applied for 10 min each. 3, 3′ diaminobenzidine (DAB kit; Dako Cytomation, Heverlee, Belgium) was used as chromogenic substrate to visualize immunolabelling, resulting in a brown precipitate.

Alpha-smooth muscle actin immunohistochemistry (IHC). Alpha-smooth muscle actin (α-SMA) expression has been used to identify activated HSCs that undergo a myofibroblastic phenotype. Immunohistochemical demonstration of the HSCs was carried out applying the primary antibody of α-SMA (Dako Cytomation, Heverlee, Belgium) in a dilution of 1/100 for 30 min at room temperature. The second layer consisted of labelled polymer-horseradish peroxidase (HRP)-anti-mouse for 30 min at room temperature. 3,3′ diaminobenzidine (DAB kit, Dako, Cytomation, Heverlee, Belgium) was used as a chromogenic substrate to visualize immunolabelling, resulting in a brown precipitate.

Microscopic evaluation. Microscopic evaluation for Sirius red, CD31, Ki67, VEGF and α-SMA was carried out blinded by two independent investigators unaware of the status of the animals. The Sirius red staining for the CBDL model was scored according to the semi-quantitative Metavir score (Bedossa & Poynard 1996). The Metavir fibrosis stage was scored as follows: F0: no fibrosis; F1: fibrotic changes confined to the portal tracts (portal fibrosis), with only mild portal expansion; F2: portal fibrosis is present with formation of few septa; F3: formation of portal-to-portal fibrous septa (septal fibrosis); F4: cirrhosis. To score the CCl_4 model, we have used another scoring method (Arezzini *et al.* 2003) to score the changes within the pericentral area: Stage

0, no fibrosis; Stage I, accumulation of collagen fibrils around the CV, but no visible extension of fibrous tissue from central venous area; Stage II, fibrous septae extending from the CV but no bridging to portal tracts or between adjacent CV; Stage III, fibrous bridging between adjacent CV or between CV and portal tracts; Stage IV, cirrhosis with hepatocellular nodules circumscribed by fibrous tissue.

Vascular density in the liver tissue was assessed by determining the count of CD31 labelled endothelial cells in five areas of the total liver lobe at 10× magnification. We have counted in each area the positive CD31 labelled blood vessels and took the sum of all five areas.

The number of proliferating endothelial cells, determined by Ki67 staining, was evaluated in 10 areas of the total liver lobe at 40× magnification. We have counted in each area the positive Ki67-labelled endothelial cells and took the sum of all 10 areas. The intensity of VEGF staining was semi-quantitatively scored as follows: 1 = <30% of hepatocytes stained, 2 = 30–70% of hepatocytes stained, 3 = >70% of hepatocytes stained.

Statistical analysis

Data were given as the mean ± standard error of the mean (SEM). A Students *t*-test, Mann–Witney *U*-test and a Kruskal–Wallis test were used to compare the different groups as appropriate. A P value of <0.05 was considered statistically significant.

Results

Characteristics of the mice models

There was no *mortality* observed in the control mice for CCl_4 or in sham-operated mice. Two out of 30 mice (5%) died after CCl_4 induction because of technical failure during injection. A mortality rate of 10% (three of 30 mice) was seen in the CBDL mice model during 6 weeks after induction. All deaths occurred in the first week after induction, which was due to bile leakage and subsequently sepsis. Preliminary experiments showed no further survival of all CBDL mice within 7–10 weeks after induction.

At laparotomy, there were no adhesions found in the CCl_4 mice, which was in contrast to the CBDL mice where sticking of the liver to the mesentery frequently occurred. Fifty percent of the CBDL mice had *ascites* after 6 weeks induction, whereas no ascites was found in the CCL_4 mice at 16 weeks.

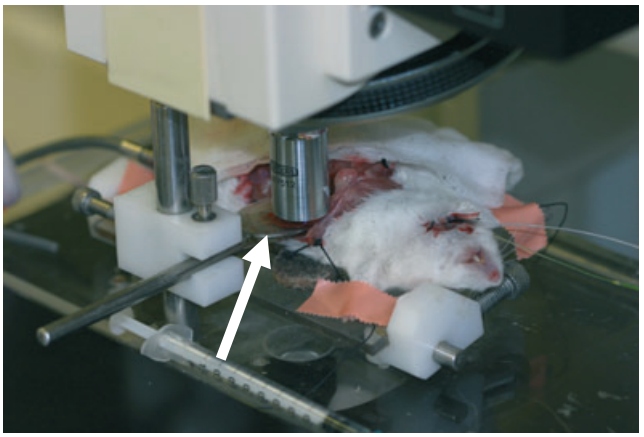

Figure 1 The intravital microscope and surgical preparation. The lower surface of the left liver lobe was situated horizontally to the microscope and the plasticine disk (white arrow) minimized the respiratory movements of the lobe.

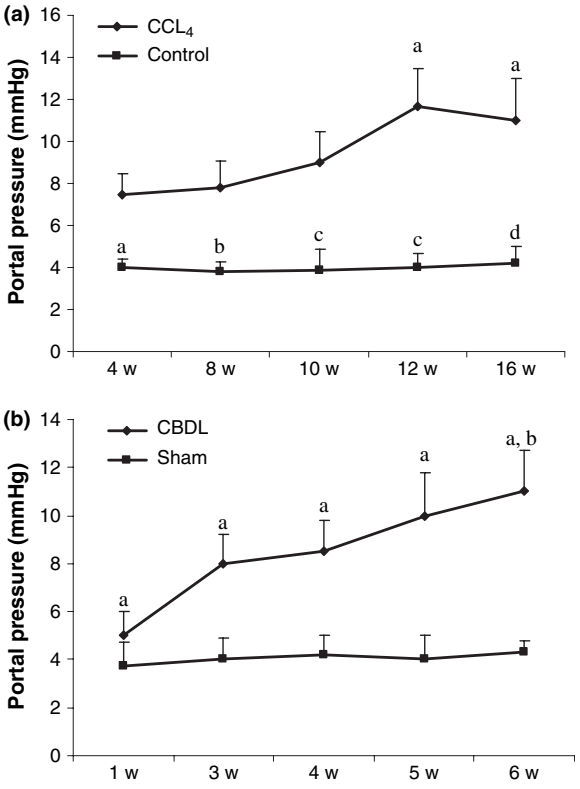

Figure 2 Portal pressures (mmHg) of control and CCl4 mice: (a) sham-operated and CBDL mice (b). Data are expressed as mean ± SEM. CCl_4: $^{a}P = 0.03$ *vs*. 4 w CCL_4, $^{b}P = 0.03$ *vs*. 8 w CCL_4, $^{c}P = 0.005$ *vs*. 10 w and 12 w CCL_4, $^{d}P = 0.05$ *vs*. 16 w CCL_4. CBDL: $^{a}P < 0.01$ *vs*. sham-operated, $^{b}P < 0.001$ *vs*. 1 w CBDL. w: weeks.

The PP measurements are shown in Figure 2. Portal pressure was significantly higher in the CCl_4 mice after 4, 8, 10, 12 and 16 weeks compared with the control group. There was a progressive increase in PP related to the duration of CCl_4 administration and the highest value was reached after 12 weeks (Figure 2a).

After CBDL induction, PP became significantly higher at 3 weeks and the highest value reached at 6 weeks compared with sham-operated mice (Figure 2b).

The MAP tended to be higher ($P = 0.08$) in the control group (115 ± 6 mmHg) compared with the CCl_4 group (98 ± 8 mmHg). In the CBDL group, MAP was significantly lower (86 ± 3 mmHg; $P = 0.02$) compared with the sham-operated group (103 ± 5 mmHg).

Microscopic findings

Sirius red staining is shown in Figure 3. CD31, Ki67, VEGF and α-SMA staining and scores are shown in Figures 4, 5 and 6 and Table 1.

CCl_4 mice. Control mice for CCl_4 did not develop any fibrotic changes on sirius red staining (Stage 0) (Figure 3a). After 8 weeks of CCl_4 administration, the liver architecture demonstrated a reversed lobulation due to the development of centro-central fibrotic linkages (Stage III), which developed further to centro-portal thin fibrotic septa after 12 weeks (Stage III to Stage IV). Although a part of this group (86%) reached the Stage IV stadium at this time, all mice at 16 weeks had homogenously the characteristics of a cirrhotic liver (Figure 3b).

Mice given CCl_4 developed a significant higher number of blood vessels located within the fibrous septa, scored on CD31 staining (Figure 4a). The number of blood vessels progressively increased with the period of CCl_4 induction, with the highest number at 16 weeks. Moreover, the proliferating endothelial cells, scored by Ki67 staining, increased after CCl_4 induction, with the highest amount at 10 weeks (Figure 4b, Table 1A).

The expression of VEGF was significantly increased after CCl_4 administration, with the highest expression at 16 weeks (Table 1A). In the control group, VEGF was detected in the first layer of hepatocytes around the central and portal venule (Figure 5a). After CCl_4 administration, VEGF was also detected in multiple layers of hepatocytes further away from the central and portal venule (Figure 5b).

Staining of α-SMA was located around the blood vessels (PV and hepatic arteries) in control mice (Figure 6a). No staining of HSC was observed along the sinusoidal wall. After 4 weeks of CCl_4 induction, increased sinusoidal wall

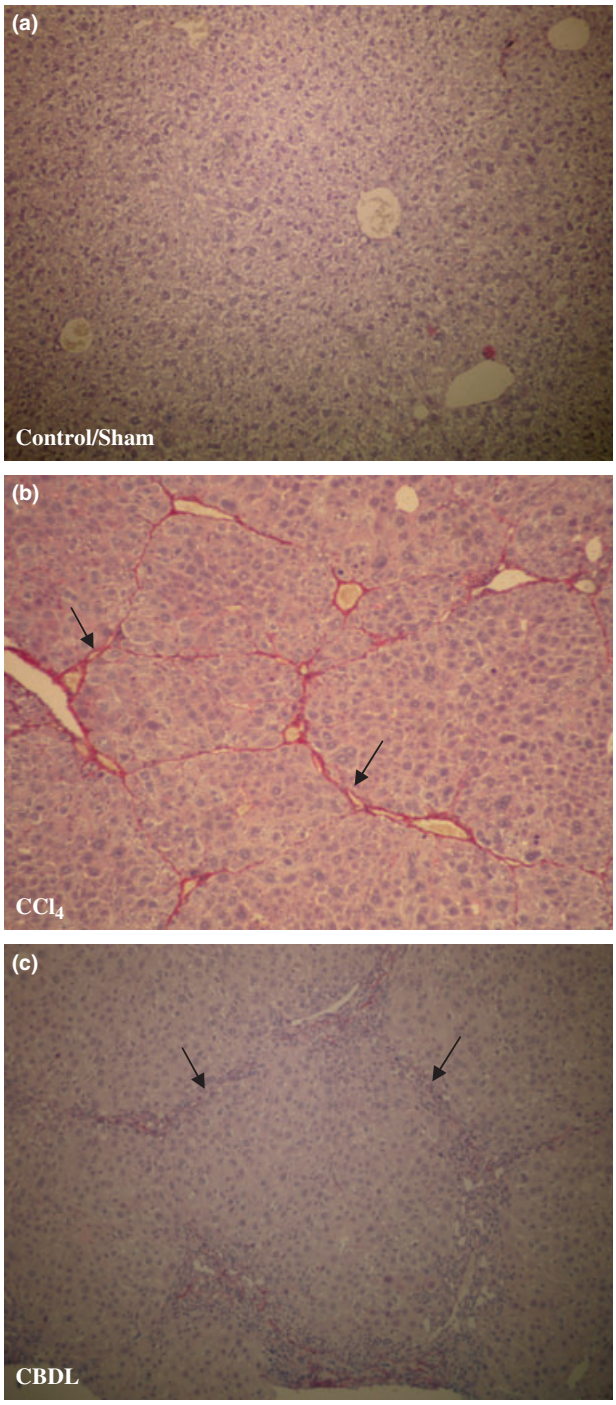

Figure 3 Sirius red staining (objective magnification 10×). (a) Control mice for CCl_4 and sham-operated mice did not develop fibrosis (Stage 0 or F0). (b) CCl_4 mice developed micronodular cirrhosis (Stage IV) after 16 weeks of CCl_4 administration (black arrow: fibrotic strands). (c) Six weeks after CBDL induction, mice developed fibrosis with nodule formation (F4) (black arrow: fibrotic strands).

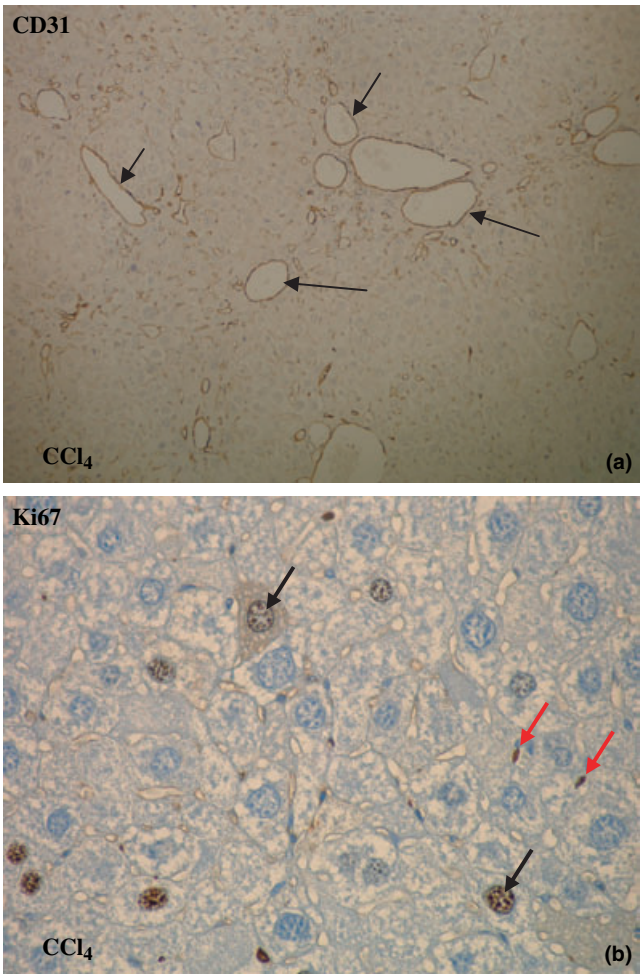

Figure 4 CD31 and Ki67 immunohistochemistry: brown staining (arrows) for endothelial cells (objective magnification 10× and 40×). (a) The number of blood vessels increased in time with the highest number of blood vessels at 16 weeks after CCl_4 administration and at 3 weeks after CBDL induction (10×). (b) The number of Ki67-positive proliferating endothelial cells increased as well after CCl_4 administration and CBDL induction (40×; red arrows: endothelial cells, black arrows: proliferating hepatocytes).

staining was apparent and related to the occurrence of spindle-shaped cells along the sinusoidal wall. They were found in groups of two or three cells surrounded by staining fibres around the central venule. After 16 weeks, the septa dissected the parenchyma with nodular transformation (Figure 6b). This phenomenon implies the transition of quiescent HSCs into activated cells during fibrosis formation.

CBDL mice. Sham-operated mice did not develop any fibrosis (F0 stadia) on sirius red staining (Figure 3a). After

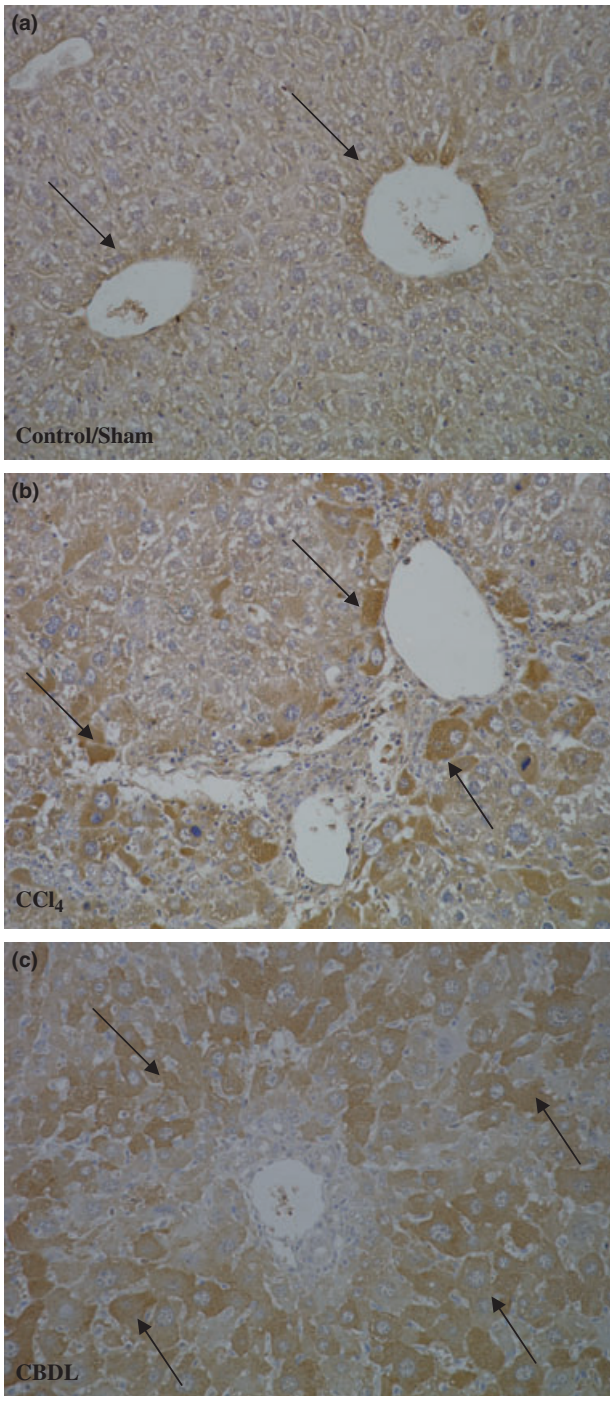

Figure 5 VEGF immunohistochemistry (objective magnification 20×). (a) In control and sham-operated mice, VEGF was detected in the first layer of hepatocytes around the venules (black arrows). (b) After CCl_4 and CBDL induction, the per centage hepatocytes that was positive increased with the highest concentration at 16 weeks for CCl_4 administration (b) and at 3 weeks for CDBL induction (c).

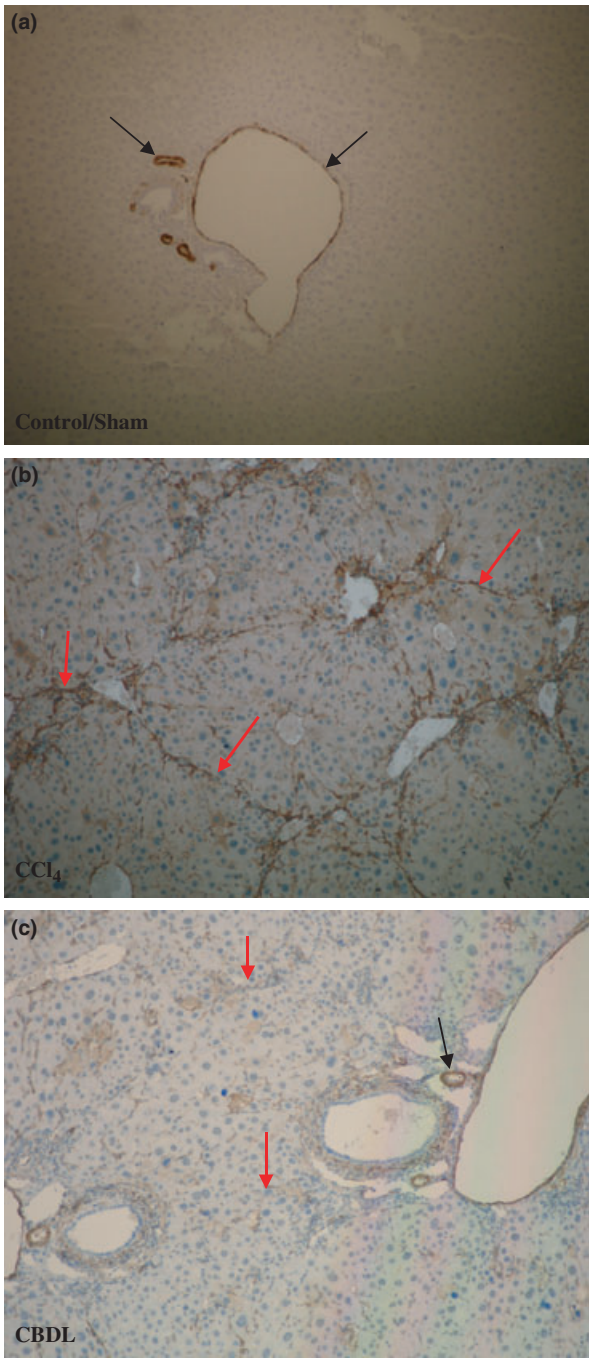

Figure 6 α-SMA immunohistohemistry (magnification 10×). (a) α-SMA expression was located around the blood vessels (portal venules and hepatic arteries; black arrows) in control and sham-operated mice. No staining of hepatic stellate cells was observed (b, c). In contrast, after induction of CCl_4 or CBDL, there was a progressive accumulation of α-SMA positive spindle-shaped cells along the sinusoidal wall within the fibrous septa in the pericentral or periportal area respectively (red arrows; hepatic artery: black arrow).

1 week of CDBL induction, mild periportal alterations were observed, described as F1. A further evolution of fibrotic changes into F2 was obtained after 3 weeks with nodular changes of the liver parenchyma (F4) at week 6 (Figure 3c).

On CD31 staining, a higher number of blood vessels was located within the fibrous septa after 1 week of CBDL induction compared with sham-operated mice, with further a progressive increase at 3 and 6 weeks. The number of proliferating endothelial cells was also significantly increased after CBDL induction, scored on Ki67 staining (Table 1B).

After 1 week of CBDL, VEGF was detected in the first layer hepatocytes around the central and portal venule, as in sham-operated mice, and additionally in multiple layers of hepatocytes further away from the central and portal venule. The highest expression of VEGF was reached at 3 weeks after CBDL induction (Figure 5c, Table 1B).

Three weeks after CBDL induction, the extend of portal tract demonstrated on α-SMA IHC an increased staining of spindle-shaped cells along the sinusoidal wall. The progression of increased α-SMA positive spindle-shaped cells paralleled the development of fibrosis to cirrhosis in the CBDL mice model (Figure 6c).

Intravital fluorescence microscopy

Data of all experimental groups are shown in Figure 7 and Table 2.

Sham-operated mice. Control mice for CCl_4 and sham-operated mice showed a normal intrahepatic microcirculation. Normal structures of PV, sinusoids, CV and a typical sinusoidal network were observed, with no additional structures like intrahepatic shunts (Figure 7a, Table 2A–B).

Sites of vitamin-A auto-fluorescence (suggesting the presence of HSC) were uniformly distributed across the acinus.

CCl_4 mice. Carbon tetrachloride cirrhotic livers had an inhomogeneous distribution of vitamin A auto-fluorescence sites with accumulation especially in zone 3 (pericentral area), where fibrosis started after CCl_4 administration. In CCl_4 mice, sinusoid-free spaces were located around the central venule, the latter being dilated compared with control mice (Figure 7b). After 4 weeks of CCl_4 induction, the diameter of the central venule increased significantly and progressively to a maximum value at 16 weeks (Table 2A). We have measured the diameter of PV in control mice, but we could not measure PV diameters in CCl_4 mice. The PV were lying deeper inside the liver tissue, prohibiting an exact measurement of the diameter. A possible explanation was the presence of fibrotic tissue in zone 3 pushing the portal tract

Table 1 CD31, Ki67 and VEGF score. Vascular density in the liver tissue was assessed by determining the count of CD31-labelled endothelial cells in five areas of the total liver lobe at 10× magnification. We have counted in each area the positive CD31-labelled blood vessels and took the sum of all five areas. The mean number of blood vessels ± SEM is given. Ki67-positive proliferating endothelial cells were counted in 10 areas of the total liver lobe at 40× magnification. The number of proliferating endothelial cells ± SEM is given. The intensity of VEGF staining was semi-quantitatively scored as follows: 1 = <30% of hepatocytes stained, 2 = 30–70% of hepatocytes stained, 3 = >70% of hepatocytes stained. The mean intensity of VEGF ± SEM is given

	Control 16 weeks (n = 4)	CCl_4 4 weeks (n = 6)	CCl_4 8 weeks (n = 6)	CCl_4 10 weeks (n = 6)	CCl_4 12 weeks (n = 6)	CCl_4 16 weeks (n = 6)
A: CCl_4*						
CD31	55.8 ± 5.6	104.3 ± 5.7[a,e]	150 ± 14.2[b,f]	135 ± 12.0[c,g]	151.5 ± 20.5[b]	205 ± 10.5[d]
Ki67	0	16.3 ± 5.3[d]	25.0 ± 6.9	47 ± 4.2[a]	31.3 ± 5.3[b]	33.7 ± 3.8[c]
VEGF	1 ± 0	2 ± 0.2[a,e]	2 ± 0.2[a,e]	2 ± 0.4[b]	2 ± 0.5[c]	3 ± 0[d]

	Sham-operated 6 weeks (n = 4)	CBDL 1 week (n = 6)	CBDL 3 weeks (n = 6)	CBDL 6 weeks (n = 6)
B: Common bile duct ligation†				
CD31	55.8 ± 5.6	80.8 ± 5.9[a,b]	181.8 ± 23.1[a]	147.8 ± 35.0[a]
Ki67	0	2 ± 0	33.7 ± 4.8[a, b]	30.0 ± 10.0
VEGF	1 ± 0	2 ± 0.2[a,b]	3 ± 0.2[a]	3 ± 0[a]

*CD31: [a]P = 0.05 *vs*. control, [b]P = 0.006 *vs*. control, [c]P = 0.011 *vs*. control, [d]P = 0.004 *vs*. control, [e]P = 0.004 *vs*. 16 weeks CCl_4, [f]P = 0.028 *vs*. 16 weeks CCl_4, [g]P = 0.010 *vs*. 16 weeks CCl_4; Ki67: [a]P = 0.007 *vs*. control, [b]P = 0.009 *vs*. control, [c]P = 0.01 *vs*. control, [d]P = 0.01 *vs*. 10 weeks; VEGF: [a]P = 0.003 *vs*. control, [b]P = 0.004 *vs*. control, [c]P = 0.016 *vs*. control, [d]P = 0.001 *vs*. control, [e]P = 0.004 *vs*. 16 weeks CCl_4.
†CD31: [a]P < 0.01 *vs*. sham-operated, [b]P = 0.001 *vs*. CBDL 3 and 6 weeks; Ki67: [a]P = 0.02 *vs*. sham-operated, [b]P = 0.02 *vs*. CBDL 1 week; VEGF: [a]P = 0.001 *vs*. sham-operated, [b]P = 0.002 *vs*. CBDL 3 and 6 weeks.

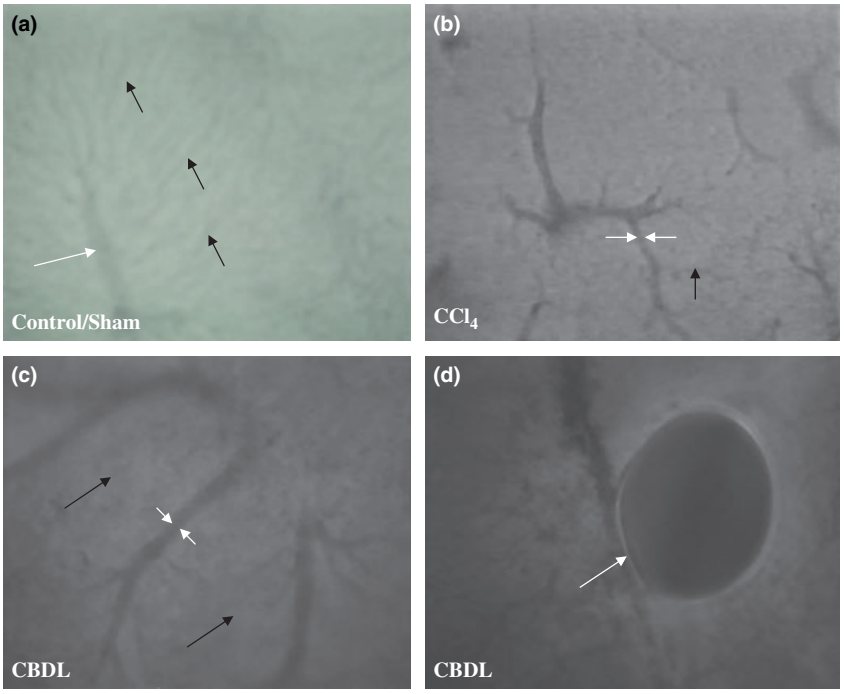

Figure 7 Intravital fluorescence microscopy (objective magnification 10× and 20×). (a) A normal hepatic microcirculation was observed in control and sham-operated mice (20×). Sinusoids (black arrow), portal venules and central venules (white arrows) had a normal structure. In contrast, a marked distortion was seen after 16 weeks of CCl_4 administration (b) (10×) and 6 weeks of common bile duct ligation (c) (10×). Sinusoidal diameter decreased and central venule or portal venule diameter respectively increased. Bile lakes (white arrow) were found in portal tracts in CBDL mice (d) (20×).

(zone 1) deeper away in the liver. With IVFM, we can only detect the upper surface of the liver. When we changed our focus, we could detect the PV, but the outline of the PV was not sharp enough to measure accurately the diameter. After CCl_4 induction, the sinusoidal diameter decreased progressively, which was correlated with a longer period of CCl_4

Table 2 Intravital microscopy observations. Diameters (μm) of sinusoids, central venules, portal venules and shunts are expressed as mean ± SEM

	Control (n = 4)	CCl_4 4 week (n = 6)	CCl_4 8 week (n = 6)	CCl_4 10 week (n = 6)	CCl_4 12 week (n = 6)	CCl_4 16 week (n = 6)
A: CCl_4*						
Sinusoidal diameter (μm)	4.15 ± 0.03	3.08 ± 0.02[a,b]	3.04 ± 0.03[a,b]	3.02 ± 0.03[a,b]	3.04 ± 0.03[a,b]	2.84 ± 0.03[a]
Central venule diameter (μm)	8.6 ± 0.4	11.9 ± 0.5[c,f,g]	10.8 ± 0.3[b,d,h]	12.7 ± 0.7[e]	14.0 ± 0.5[a]	13.6 ± 0.6[a]
Shunt diameter (μm)	Not observed	15.1 ± 1.0[b,i]	14.9 ± 0.6[b,j]	15.6 ± 0.7[b,k]	18.3 ± 0.8[l]	22.2 ± 1.1

	Sham-operated 6 week (n = 4)	CBDL 1 week (n = 6)	CBDL 3 week (n = 6)	CBDL 6 week (n = 6)
B: CBDL†				
Sinusoidal diameter (μm)	4.35 ± 0.09	4.64 ± 0.11	4.00 ± 0.13[a,c]	3.7 ± 0.05[b,c]
Central venule diameter (μm)	9.7 ± 1.0	10.1 ± 1.2[d]	8.1 ± 1.5[e]	13.0 ± 2.9
Portal venule diameter (μm)	11.0 ± 1.1	10.5 ± 0.8[g]	26.0 ± 2.4[f,g]	15.9 ± 3.2
Shunt diameter (μm)	Not observed	Not observed	22.3 ± 5.1	16.2 ± 6.1

*[a]P < 0.001 *vs.* control; [b]P < 0.001 *vs.* 16 week CCl_4; [c]P = 0.007 *vs.* control; [d]P = 0.010 *vs.* control; [e] P = 0.002 *vs.* control; [f]P = 0.005 *vs.* 12 w CCl_4; [g]P = 0.034 *vs.* 16 week CCl_4; [h]P < 0.001 *vs.* 12 week CCl_4; [i]P = 0.018 *vs.* 12 week CCl_4; [j]P = 0.003 *vs.* 12 week CCl_4; [k]P = 0.025 *vs.* 12 week CCl_4; [l]P = 0.017 *vs.* 16 week CCl_4.

†[a]P = 0.001 *vs.* sham-operated; [b]P < 0.001 *vs.* sham-operated; [c]P = 0.001 *vs.* CBDL 1 week; [d]P = 0.05 *vs.* sham-operated; [e]P = 0.015 *vs.* sham-operated; [f]P = 0.04 *vs.* sham-operated; [g]P = 0.02 *vs.* CBDL 6 week.

induction and appearance of cirrhosis (Figure 7b, Table 2A). Intrahepatic shunts developed gradually after CCl_4 induction, with a significant increase in diameter and number when the mice became cirrhotic (12 and 16 weeks) (Table 2A). Blood in the shunts flowed from the portal tract (zone 1) to the central venule (zone 3), the site of fibrosis, where we also identified the accumulation of vitamin A auto-fluorescence HSC. After a longer CCl_4 induction period, we detected less auto-fluorescent accumulation in HSC, which indicated a loss of vitamin A storage in activated HSC.

CBDL mice. In the CBDL model, sticking of the liver to the mesentery occurred frequently, which complicated the preparation of the liver for IVFM. The liver was carefully released from the mesentery, which gave sometimes little bleedings. Then, the lower surface of the liver was placed horizontally to the microscope with the most precaution.

In contrast to sham-operated mice, the hepatic microcirculation was markedly disturbed in CBDL mice (Figure 7c). After 1 week of CBDL induction, periportal (zone 1) changes were observed, with no clearly visualized sinusoids and an accumulation of vitamin A auto-fluorescence sites. After 3 weeks of CBDL induction, the microcirculatory changes were more pronounced. Diameters of portal and CV were significantly enlarged and the sinusoidal diameter was significantly narrowed compared with sham-operated mice (Table 2B). Sinusoidal-free spaces were located around PV and furthermore intrahepatic shunts developed gradually, bypassing sinusoids and draining blood from the portal to the central venule. Six weeks after CBDL induction, diameters of sinusoids diminished significantly. Furthermore, CV and PV diameters remained significantly higher compared with sham-operated mice (Table 2B). Another remarkable appearance was the presence of bile lakes in the portal tracts (Figure 7d). IVFM is not an adequate technique for bile flow measurements.

Discussion

The present study is the first *in vivo* study comparing hepatic microcirculatory changes in relation to fibrotic alterations and angiogenesis in two different cirrhotic *mice* models. The validation of mice models instead of rat models has a lot of advantages in molecular biology and can be used for genetically modified animals (e.g. transgenic or knock-out mice). The technique of IVFM has the advantage, in comparison with traditionally used scanning electron microscopy and IHC, to study dynamic alterations in the hepatic microcirculation.

A number of models of cirrhosis have been described, but the *intraperitoneal* CCL_4 model has been most widely used for the study of the intrahepatic microcirculation. Intraperitoneal injection can lead to damage and adherences among the mesentery, bowel and liver, which subsequently limits the possibilities to perform *in vivo* experiments in the

abdominal cavity, e.g. flow measurements and intravital microscopy studies. Therefore, we have validated a *subcutaneously* induced CCL_4 model (Geerts AM, Vanheule E, Praet M, Van Vlierberghe H, De Vos M, Colle I, 2008, unpublished data), which is an experimental model for micronodular cirrhosis, that mimics the characteristics of human alcoholic cirrhosis. Cirrhosis develops after 16 weeks of *subcutaneous* CCl_4 injection and is associated with a parallel increase in portal pressure.

Other advantages of a *subcutaneously* induced CCl_4 mice model are the minimal side-effects and lower mortality rate than CCl_4 mice models induced by inhalation or intraperitoneal injection. However, the duration of the development of cirrhosis (16 weeks) is much longer (Lieber 1984). Inhalation of CCL_4 might cause potential health hazards for the investigator and can lead to toxicity of other organs like kidney, lung, brain and spleen (Sinicrope *et al.* 1984; Benson *et al.* 2001). Intraperitoneal injection can also lead to toxicity of the kidney (Zimmerman *et al.* 1983).

The CBDL model is a model for secondary biliary cirrhosis, which is less frequently seen in clinic than human alcoholic cirrhosis. The CBDL model has a high mortality rate and can also lead to damage and adherences of the mesentery, bowel and liver, which complicate *in vivo* experiments in the abdominal cavity. In contrary to the CCl_4 model, the CBDL model leads to cirrhosis in 6 weeks, which is also observed in clinic, where cirrhosis can develop very quickly after bile duct obstruction. Other models for cirrhosis such as thioacetamide (Popov *et al.* 2006) and dimethylnitrosamine (Abraldes *et al.* 2006) are available, but they will not be further discussed in detail.

In a healthy liver, the sinusoids with regular diameter are a continuous network organized to form an acinus. With IVFM and with histology, we can see that the intrahepatic architecture is totally disturbed after CCl_4 and CDBL induction, with the complete loss of the zonation in the liver.

The architectural microvascular changes in the CCl_4 model are situated in zone 3 (pericentral area), which is the site for drug metabolism and is sensitive to ischaemic and toxic damage including alcohol and CCl_4 (Lieber 1984; Sato & Nakajima 1984; Koop & Coon 1986; Zimmerman 1986; Garro & Lieber 1990; Koop & Tierney 1990). There are marked sinusoidal-free spaces predominantly around the CV, which are enlarged, and is associated with accumulation of HSC in zone 3. These features have also been found in the CCl_4 rat (Vollmar *et al.* 1998). In contrast to the CCl_4 mice, microvascular changes occur in zone 1 (periportal area) in the CBDL model. There are marked sinusoidal-free spaces around the PV, which are enlarged. Additionally, bile lakes are observed in the CBDL mice.

At the stage of cirrhosis, a marked distortion and narrowing of the sinusoids are observed in both mice models which increase the intrahepatic resistance, described in previous studies (Pinzani 1995; Rockey 1997). Several mechanisms can be responsible for the identified alterations of sinusoidal perfusion: (i) accumulation of fibrotic tissue can cause narrowing of the sinusoids, (ii) cirrhotic animals exhibit activation of HSCs with release of vasoactive substances, e.g. endothelin-1 and carbon monoxide, that cause changes in sinusoidal diameter at locations where HSC reside (Zhang *et al.* 1994; Suematsu *et al.* 1995; Rockey 1997); (iii) subsequent to CBDL, intrahepatic bile ductules and canaliculi become dilated and periportal oedema develops (Edlund & Gelin 1962; Koeppel *et al.* 1997; Ito *et al.* 2003). Therefore, sinusoidal narrowing can result from increased hydrostatic pressure in the biliary tract and account for sinusoidal flow disturbances in the present study, (iv) increased numbers of leucocytes and hepatic macrophages are found after CBDL. These inflammatory cells can also alter the sinusoidal diameter. This impaired sinusoidal perfusion can further aggravate liver injury by decreasing tissue oxygenation and energy supply as well as the removal of toxic metabolites.

Hepatic stellate cells exhibit an activated phenotype in liver disease and, among other features, acquire contractile properties by which HSCs contribute to the regulation of sinusoidal blood flow and vascular resistance. They also synthesize α-SMA, extracellular matrix proteins and collagen. The first consequence is the cappilarization of the sinusoids that lose their fenestrae, develop a basement membrane and become more rigid, which impairs the metabolic exchange with the hepatocytes and increases mechanically the sinusoidal vascular resistance. The active contraction of HSC further increases the hepatic vascular tone and contributes to the development of portal hypertension (Pinzani & Gentilini 1999; Bataller *et al.* 2003).

As we have shown on α-SMA staining, the progression of increased α-SMA positive spindle-shaped cells paralleled the development of fibrosis to cirrhosis in both mice models, which demonstrates the presence of activated HSCs during the development of cirrhosis. The presence of activated HSCs appears in the pericentral area (zone 3) for the CCl_4 model and in the periportal area (zone 1) for the CBDL model, which are respectively the zones where fibrosis first occurs. These findings are also confirmed by our observations of vitamin A distribution with IVFM.

In parallel with this sinusoidal remodelling, there is a process of angiogenesis, in which HSCs play a major role, such as the production of angiogenic growth factors (e.g. VEGF). Angiogenesis occurs mainly along areas of active inflammation and fibrous septa and probably favours

inflammation, tissue repair and gives rise to intrahepatic shunts.

Vascular endothelial growth factor, one of the proteins responsible for new blood vessel formation, is significantly increased during the course of liver fibrosis/cirrhosis in the present study and confirms the results of other experimental studies (Corpechot *et al.* 2002). VEGF exhibits major biological activities, such as growth and proliferation of endothelial cells, all of which contribute to the induction of angiogenesis (Carmeliet 2005). It is possible that hepatocytes, in a continuously damaged liver (e.g. after CCl_4 and CBDL induction), are in a sustained hypoxic state that strongly upregulates VEGF transcription and protein synthesis (El-Assal *et al.* 1998). This VEGF production in the hypoxic area of the liver, can further lead to the activation and proliferation of endothelial cells, which finally results in the formation of newly formed blood vessels or shunts, that are necessary to restore the intrahepatic blood circulation. Models of liver regeneration have shown that HSC also produce VEGF, above extracellular matrix components and TGF-β, and play a role in hepatic angiogenesis (Fausto 2000; Wack *et al.* 2001; Lee *et al.* 2007). We further have to investigate the role of hypoxia as the inducible factor of VEGF in both cirrhotic models. We did not find any studies about angiogenesis and toxicity of CCl_4 in other organs like kidney, brain and lung.

The role of angiogenesis in liver pathology is also demonstrated in clinical studies: in patients with hepatocellular carcinoma (Papetti & Herman 2002; Zhang *et al.* 2006) and in human cirrhotic livers from patients with chronic hepatitis C, autoimmune hepatitis, primary biliary cirrhosis and primary sclerosing cholangitis, which showed an overexpression of many key genes, such as growth factors and their receptors (VEGF, HGF, TGF-β,…) involved in the different phases of angiogenesis (Shackel *et al.* 2001, 2002). All these data suggest that angiogenesis plays a major role during liver damage and recovery.

On Ki67 IHC, we observed an increase in proliferating endothelial cells, which is probably induced by the upregulation of VEGF and other growth factors, such as HGF and TFG-β (Yancopoulos *et al.* 2000; Conway & Carmeliet 2003). We also confirmed the formation of new blood vessels on CD31 IHC, where we see a parallel increase in blood vessel amount after induction of cirrhosis in both mice models. These blood vessels are located around and in the fibrotic areas, which are probably hypoxic, suggesting that these blood vessels have to compensate the insufficient blood flow in the liver.

Another particular feature of the hepatic angio-architecture, after CCl_4 and CBDL induction that we observe on IVFM, is the appearance of intrahepatic shunts. These vessels are large in diameter and flow from the PV to CV, bypassing the sinusoids. This could lead to liver dysfunction due to lower delivery of nutritive blood flow and the restriction of free interchange between hepatocytes and the sinusoids. These IVFM results confirm our *in vitro* results, where we have detected an increase in proliferating endothelial cells and subsequently an increase in blood vessels, probably in response to an upregulated VEGF production.

The development of shunts involves either the opening of preformed channels or the formation of new vessels or angiogenesis (Rappaport *et al.* 1983). The role of angiogenesis during the development of cirrhosis is still unclear. Whether it plays a beneficial role to control the portal pressure or exerts an additional pathogenic mechanism remains a matter of debate. It is reasonable to deduce that the fibrotic tissue around the central venule (zone 3) for the CCl_4 model and around the portal tracts (zone 1) for the CBDL model serves as a perivenular fibrotic dam that causes the obliteration and/or collapse of sinusoidal openings with subsequent redistribution of blood flow favouring low hindrance pathways, i.e. fast sinusoids or intrahepatic shunts. Our results of IVFM are conform to similar *in vivo* experiments in a CCl_4 rat model (Sherman *et al.* 1990; Vollmar *et al.* 1998; Onori *et al.* 2000), a CCl_4 mouse model induced by intraperitoneal injection (Niggemann *et al.* 2004) and a CBDL rat model described by Edlund and Gelin (1962).

In conclusion, the present study describes for the first time an *in vivo* analysis of the dynamic intrahepatic microcirculatory disturbances by IVFM in two cirrhotic *mice* models induced by *subcutaneous* administration of CCl_4 and common bile duct ligation, in relationship to consecutive stages of liver fibrosis and cirrhosis. This study provides evidence for an increasing importance of intrahepatic vascular alterations (such as shunt formation) and angiogenesis during fibrogenesis/cirrhogenesis which may be the consequence but may also contribute to the underlying process of fibrosis. We have demonstrated an upregulation of VEGF expression which may be one of the stimulating factors of angiogenesis.

Acknowledgements

The authors thank technician Julien Dupont, Ghent University Hospital for his expert technical assistance. This work is supported by a grant from Astra Zeneca Belgium, Novartis Belgium, Roche Belgium, Schering-Plough Belgium and UCB Belgium. Eline Vanheule is sponsored by a grant from Bijzonder Onderzoeksfonds (BOF-01107005).

References

Abraldes J.G., Pasarin M., Garcia-Pagan J.C. (2006) Animal models of portal hypertension. *World J. Gastroenterol.* **12**, 6577–6584.

Anthony P.P., Ishak K.G., Nayak N.C., Poulsen H.E., Scheuer P.J., Sobin L.H. (1977) The morphology of cirrhosis: definition, nomenclature, and classification. *Bull. World Health Organ.* **55**, 521–540.

Arezzini B., Lunghi B., Lungarella G., Gardi C. (2003) Iron overload enhances the development of experimental liver cirrhosis in mice. *Int. J. Biochem. Cell Biol.* **35**, 486–495.

Bataller R., Sancho-Bru P., Gines P. *et al.* (2003) Activated human hepatic stellate cells express the renin-angiotensin system and synthesize angiotensin II. *Gastroenterology* **125**, 117–125.

Bedossa P. & Poynard T. (1996) An algorithm for the grading of activity in chronic hepatitis C. The METAVIR Cooperative Study Group. *Hepatology* **24**, 289–293.

Benson J.M., Tibbetts B.M., Thrall K.D., Springer D.L. (2001) Uptake, tissue distribution, and fate of inhaled carbon tetrachloride: comparison of rat, mouse, and hamster. *Inhal. Toxicol.* **13**, 207–217.

Camussi G., Montrucchio G., Lupia E., Soldi R., Comoglio P.M., Bussolino F. (1997) Angiogenesis induced in vivo by hepatocyte growth factor is mediated by platelet-activating factor synthesis from macrophages. *J. Immunol.* **158**, 1302–1309.

Carmeliet P. (2005) Angiogenesis in life, disease and medicine. *Nature* **438**, 932–936.

Castaneda B., Debernardi-Venon W., Bandi J.C. *et al.* (2000) The role of portal pressure in the severity of bleeding in portal hypertensive rats. *Hepatology* **31**, 581–586.

Colombato L.A., Albillos A., Groszmann R.J. (1992) Temporal relationship of peripheral vasodilatation, plasma volume expansion and the hyperdynamic circulatory state in portal-hypertensive rats. *Hepatology* **15**, 323–328.

Conway E.M. & Carmeliet P. (2003) Cardiovascular biology: signalling silenced. *Nature* **425**, 139–141.

Corpechot C., Barbu V., Wendum D. *et al.* (2002) Hypoxia-induced VEGF and collagen I expressions are associated with angiogenesis and fibrogenesis in experimental cirrhosis. *Hepatology* **35**, 1010–1021.

Edlund Y. & Gelin L.E. (1962) Microcirculatory alterations in biliary obstruction. *Acta. Pathol. Microbiol. Scand.* **54**, 181–189.

El-Assal O.N., Yamanoi A., Soda Y. *et al.* (1998) Clinical significance of microvessel density and vascular endothelial growth factor expression in hepatocellular carcinoma and surrounding liver: possible involvement of vascular endothelial growth factor in the angiogenesis of cirrhotic liver. *Hepatology* **27**, 1554–1562.

Fausto N. (2000) Liver regeneration. *J. Hepatol.* **32**, 19–31.

Fernandez M., Vizzutti F., Garcia-Pagan J.C., Rodes J., Bosch J. (2004) Anti-VEGF receptor-2 monoclonal antibody prevents portal-systemic collateral vessel formation in portal hypertensive mice. *Gastroenterology* **126**, 886–894.

Garro A.J. & Lieber C.S. (1990) Alcohol and cancer. *Annu. Rev. Pharmacol. Toxicol.* **30**, 219–249.

Gaudio E., Pannarale L., Onori P., Riggio O. (1993) A scanning electron microscopic study of liver microcirculation disarrangement in experimental rat cirrhosis. *Hepatology* **17**, 477–485.

Gressner A.M. (1992) Hepatic fibrogenesis: the puzzle of interacting cells, fibrogenic cytokines, regulatory loops, and extracellular matrix molecules. *Z. Gastroenterol.* **30**(Suppl. 1), 5–16.

Gressner A.M. & Bachem M.G. (1995) Molecular mechanisms of liver fibrogenesis–a homage to the role of activated fat-storing cells. *Digestion* **56**, 335–346.

Hyytiainen M., Penttinen C., Keski-Oja J. (2004) Latent TGF-beta binding proteins: extracellular matrix association and roles in TGF-beta activation. *Crit. Rev. Clin. Lab. Sci.* **41**, 233–264.

Ito Y., Bethea N.W., Baker G.L., McCuskey M.K., Urbaschek R., McCuskey R.S. (2003) Hepatic microcirculatory dysfunction during cholestatic liver injury in rats. *Microcirculation* **10**, 421–432.

Katsuta Y., Zhang X.J., Ohsuga M. *et al.* (2005) Hemodynamic features of advanced cirrhosis due to chronic bile duct ligation. *J. Nippon Med. Sch.* **72**, 217–225.

Koeppel T.A., Trauner M., Baas J.C. *et al.* (1997) Extrahepatic biliary obstruction impairs microvascular perfusion and increases leukocyte adhesion in rat liver. *Hepatology* **26**, 1085–1091.

Koop D.R. & Coon M.J. (1986) Ethanol oxidation and toxicity: role of alcohol P-450 oxygenase. *Alcohol. Clin. Exp. Res.* **10**, 44S–49S.

Koop D.R. & Tierney D.J. (1990) Multiple mechanisms in the regulation of ethanol-inducible cytochrome P450IIE1. *Bioessays* **12**, 429–435.

Kountouras J., Billing B.H., Scheuer P.J. (1984) Prolonged bile duct obstruction: a new experimental model for cirrhosis in the rat. *Br. J. Exp. Pathol.* **65**, 305–311.

Lee S.S., Braillon A., Girod C., Geoffroy P., Lebrec D. (1986a) Haemodynamic rebound phenomena after abrupt cessation of propranolol therapy in portal hypertensive rats. *J. Hepatol.* **3**, 38–41.

Lee S.S., Girod C., Braillon A., Hadengue A., Lebrec D. (1986b) Hemodynamic characterization of chronic bile duct-ligated rats: effect of pentobarbital sodium. *Am. J. Physiol.* **251**, G176–G180.

Lee J.S., Semela D., Iredale J., Shah V.H. (2007) Sinusoidal remodeling and angiogenesis: A new function for the liver-specific pericyte? *Hepatology* **45**, 817–825.

Lieber C.S. (1984) Alcohol and the liver: 1984 update. *Hepatology* **4**, 1243–1260.

Niggemann P., Murata S., Naito Z., Kumazaki T. (2004) A comparative study of the microcirculatory changes in the developing liver cirrhosis between the central and peripheral parts of the main lobe in mice. *Hepatol. Res.* **28**, 41–48.

Onori P., Morini S., Franchitto A., Sferra R., Alvaro D., Gaudio E. (2000) Hepatic microvascular features in experimental cirrhosis: a structural and morphometrical study in CCl4-treated rats. *J. Hepatol.* **33**, 555–563.

Papetti M. & Herman I.M. (2002) Mechanisms of normal and tumor-derived angiogenesis. *Am. J. Physiol.* **282**, C947–C970.

Perez Tamayo R. (1983) Is cirrhosis of the liver experimentally produced by CCl4 and adequate model of human cirrhosis? *Hepatology* **3**, 112–120.

Pinzani M. (1995) Hepatic stellate (ITO) cells: expanding roles for a liver-specific pericyte. *J. Hepatol.* **22**, 700–706.

Pinzani M. & Gentilini P. (1999) Biology of hepatic stellate cells and their possible relevance in the pathogenesis of portal hypertension in cirrhosis. *Semin. Liver Dis.* **19**, 397–410.

Popov Y., Patsenker E., Bauer M., Niedobitek E., Schulze-Krebs A., Schuppan D. (2006) Halofuginone induces matrix metalloproteinases in rat hepatic stellate cells via activation of p38 and NFkappaB. *J. Biol. Chem.* **281**, 15090–15098.

Popper H. (1977) Pathologic aspects of cirrhosis. A review.. *Am. J. Pathol.* **87**, 228–264.

Proctor E. & Chatamra K. (1982) High yield micronodular cirrhosis in the rat. *Gastroenterology* **83**, 1183–1190.

Rappaport A.M., MacPhee P.J., Fisher M.M., Phillips M.J. (1983) The scarring of the liver acini (Cirrhosis). Tridimensional and microcirculatory considerations. *Virchows Arch. A Pathol. Anat. Histopathol.* **402**, 107–137.

Rockey D. (1997) The cellular pathogenesis of portal hypertension: stellate cell contractility, endothelin, and nitric oxide. *Hepatology* **25**, 2–5.

Rosen E.M., Lamszus K., Laterra J., Polverini P.J., Rubin J.S., Goldberg I.D. (1997) HGF/SF in angiogenesis. *Ciba Found. Symp.* **212**, 215–226; discussion 227–229.

Ruiz-Ortega M., Rodriguez-Vita J., Sanchez-Lopez E., Carvajal G., Egido J. (2007) TGF-beta signaling in vascular fibrosis. *Cardiovasc. Res.* **74**, 196–206.

Sato A. & Nakajima T. (1984) Dietary carbohydrate-and ethanol-induced alteration of the metabolism and toxicity of chemical substances. *Nutr. Cancer* **6**, 121–132.

Schaffner F. & Poper H. (1963) Capillarization of hepatic sinusoids in man. *Gastroenterology* **44**, 239–242.

Shackel N.A., McGuinness P.H., Abbott C.A., Gorrell M.D., McCaughan G.W. (2001) Identification of novel molecules and pathogenic pathways in primary biliary cirrhosis: cDNA array analysis of intrahepatic differential gene expression. *Gut* **49**, 565–576.

Shackel N.A., McGuinness P.H., Abbott C.A., Gorrell M.D., McCaughan G.W. (2002) Insights into the pathobiology of hepatitis C virus-associated cirrhosis: analysis of intrahepatic differential gene expression. *Am. J. Pathol.* **160**, 641–654.

Sherman I.A., Pappas S.C., Fisher M.M. (1990) Hepatic microvascular changes associated with development of liver fibrosis and cirrhosis. *Am. J. Physiol.* **258**, H460–H465.

Silvagno F., Follenzi A., Arese M. *et al.* (1995) In vivo activation of met tyrosine kinase by heterodimeric hepatocyte growth factor molecule promotes angiogenesis. *Arterioscler. Thromb. Vasc. Biol.* **15**, 1857–1865.

Sinicrope R.A., Gordon J.A., Little J.R., Schoolwerth A.C. (1984) Carbon tetrachloride nephrotoxicity: a reassessment of pathophysiology based upon the urinary diagnostic indices. *Am. J. Kidney Dis.* **3**, 362–365.

Suematsu M., Oda M., Suzuki H. *et al.* (1993) Intravital and electron microscopic observation of Ito cells in rat hepatic microcirculation. *Microvasc. Res.* **46**, 28–42.

Suematsu M., Goda N., Sano T. *et al.* (1995) Carbon monoxide: an endogenous modulator of sinusoidal tone in the perfused rat liver. *J. Clin. Invest.* **96**, 2431–2437.

Vollmar B., Siegmund S., Menger M.D. (1998) An intravital fluorescence microscopic study of hepatic microvascular and cellular derangements in developing cirrhosis in rats. *Hepatology* **27**, 1544–1553.

Vorobioff J., Bredfeldt J.E., Groszmann R.J. (1984) Increased blood flow through the portal system in cirrhotic rats. *Gastroenterology* **87**, 1120–1126.

Wack K.E., Ross M.A., Zegarra V., Sysko L.R., Watkins S.C., Stolz D.B. (2001) Sinusoidal ultrastructure evaluated during the revascularization of regenerating rat liver. *Hepatology* **33**, 363–378.

Yancopoulos G.D., Davis S., Gale N.W., Rudge J.S., Wiegand S.J., Holash J. (2000) Vascular-specific growth factors and blood vessel formation. *Nature* **407**, 242–248.

Yoshiji H., Kuriyama S., Yoshii J. *et al.* (2003) Vascular endothelial growth factor and receptor interaction is a prerequisite for murine hepatic fibrogenesis. *Gut* **52**, 1347–1354.

Zhang J.X., Pegoli W. Jr, Clemens M.G. (1994) Endothelin-1 induces direct constriction of hepatic sinusoids. *Am. J. Physiol.* **266**, G624–G632.

Zhang Z.L., Liu Z.S., Sun Q. (2006) Expression of angiopoietins, Tie2 and vascular endothelial growth factor in angiogenesis and progression of hepatocellular carcinoma. *World J. Gastroenterol.* **12**, 4241–4245.

Zimmerman H.J. (1986) Effects of alcohol on other hepatotoxins. *Alcohol. Clin. Exp. Res.* **10**, 3–15.

Zimmerman S.W., Norback D.H., Powers K. (1983) Carbon tetrachloride nephrotoxicity in rats with reduced renal mass. *Arch. Pathol. Lab. Med.* **107**, 264–269.

